Assessment of Dual Plane PIV Measurements in Wall Turbulence Using DNS Data

N. Saikrishnan, I. Marusic, E.K. Longmire

Abstract Experimental dual plane particle image velocimetry (PIV) data are assessed using direct numerical simulation (DNS) data of a similar flow with the aim of studying the effect of averaging within the interrogation window. The primary reason for the use of dual plane PIV is that the entire velocity gradient tensor and hence the full vorticity vector can be obtained. One limitation of PIV is the limit on dynamic range, while DNS is typically limited by the Reynolds number of the flow. In this study, the DNS data are resolved more finely than the PIV data, and an averaging scheme is implemented on the DNS data of similar Re_τ to compare the effects of averaging inherent to the present PIV technique. The focus here is to identify vortex core distributions for which the two-dimensional and three-dimensional swirl strengths are used. The studies are performed in the logarithmic region of a turbulent boundary layer at a location of 110 wall units from the wall. The dual plane PIV data are measured in a zero pressure gradient flow over a flat plate at Re_τ of 1160, while the DNS data are extracted from a channel flow at Re_τ of 934. Statistical tools suggest the presence of hairpin shaped vortex structures, and the effects of averaging are quantified. It is observed that the effects of averaging are small compared to the raw DNS data with excellent agreement for a variety of vortex core angle statistics. The results indicate that the present PIV technique is an accurate and very reliable method for the purposes of statistical analysis and identification of vortex structures.

1
Introduction

A fundamental problem in the study of dynamics of turbulent boundary layers has been in understanding the relation between vortex structures and Reynolds shear stress. Wall turbulence studies, both experimental and computational, have yielded a variety of results and models. Various studies have been directed towards understanding the eddy structures within the turbulent boundary layer. The concept of 'hairpin vortices' was first introduced by Theodorsen[12] and are now widely accepted to be a primary feature of wall turbulence[1]. Adrian, Meinhart & Tomkins[2] experimentally observed spatially coherent groups of hairpin vortices in the logarithmic and outer wake layers of turbulent boundary layers. The authors termed such a group of coherent hairpin vortices a "hairpin packet". Ganapathisubramani, Longmire & Marusic[7] recently showed with stereoscopic PIV data that these packets occupy a relatively small percentage of the total area but contribute significantly to the total Reynolds shear stress generated. Hence, hairpin packets play a very important role in the production of turbulence and transport of momentum. Various studies, numerical and experimental, have been directed towards better understanding the shape, size, orientation and dynamics of these structures.

Dual plane PIV is a novel technique where the complete velocity gradient tensor can be determined experimentally. It has been successfully used for measurements in the turbulent boundary layer by Kahler[8] and Ganapathisubramani, Longmire, Marusic & Pothos[5]. Dual plane PIV involves the measurement of three velocity components in one wall parallel plane using stereo PIV and two or three velocity components in a parallel plane separated by a small distance using conventional or stereo PIV. Either setup provides the complete velocity gradient tensor for incompressible flows, and hence the complete vorticity vector. This can be used for analyzing structures in the turbulent boundary layer.

In PIV, the velocity vector in each interrogation window is calculated by means of a cross-correlation algorithm where the displacements of all the particles within the interrogation window are taken into consideration. Scales smaller than the size of the interrogation window are averaged within the window, and a representative velocity is associated with each interrogation window. The resolution of the velocity field depends on the experimental setup, but in general this might be affected by practical issues such as seeding and zooming in on the interrogation volume. One main limitation of PIV in general is the minimum resolution attainable.

Direct numerical simulation (DNS) is a commonly used numerical technique to study structures in turbulent

N. Saikrishnan, I. Marusic, E.K. Longmire, Department of Aerospace Engineering & Mechanics, University of Minnesota, Minneapolis, MN 55414, USA

Correspondence to:
E.K. Longmire, Department of Aerospace Engineering & Mechanics,
107 Akerman Hall, 110 Union St. SE, University of Minnesota, Minneapolis, MN 55414, USA
Email: ellen@aem.umn.edu

flows. Kim, Moin & Moser[9] used DNS to obtain turbulent statistics in a fully-developed channel flow. However, DNS is limited by the Reynolds number of flow, since the Reynolds number directly influences the range of scales in the problem, as discussed by Moin & Mahesh[10]. Recently, del Álamo, Jiménez, Zandonade & Moser[3] performed direct numerical simulations at friction Reynolds numbers Re_τ of up to 1900 in a channel flow.

In the present study, the aim is to be able to quantify and assess the effects of averaging which might be introduced as a result of the cross-correlation technique of PIV. To be able to do this, a DNS dataset of comparable Re_τ is utilized. The resolution of the DNS dataset is finer than the PIV dataset; hence smaller scales can be resolved in the DNS. In order to understand the effects of averaging, the DNS dataset is averaged to the resolution of the PIV dataset. The statistics and instantaneous velocity fields are compared between the raw and the averaged DNS datasets. The statistics from the different datasets yield vortex core angle distributions, which can be used to understand the characteristics of structures in the turbulent boundary layer and to understand the shortcomings, if any, of the experimental technique as compared to the numerical technique.

The comparison between the PIV and the DNS data is made in the logarithmic region of the turbulent boundary layer. In spite of the fact that both these studies are conducted at similar Re_τ, they are fundamentally different flow situations. The PIV studies are made in the zero pressure gradient boundary layer over a flat plate, whereas the DNS is performed in a channel flow. However, it is expected that in the logarithmic region, the effect of the opposing wall of the channel will be negligible and hence the structures observed in the channel flow will approximate those in a developing boundary layer. This assumption may not hold at larger distances from the wall and care has to be taken to extend this argument to the entire boundary layer.

The paper is organized as follows. In section 2, the experimental setup and the DNS dataset are briefly described. In section 3, the averaging technique is described and its variations are discussed. In section 4, the results obtained from the raw and the averaged DNS are described in comparison with the PIV. In section 5, the vorticity vector is used to study the characteristics of structures in the boundary layer. In section 6, conclusions and scope for further work are discussed.

2
Description of PIV and DNS datasets

The dual plane particle image velocimetry (PIV) dataset was obtained from experiments conducted in a suction-type boundary layer wind tunnel by Ganapathisubramani[6]. Measurement planes were located 3.3 m downstream of a trip wire in a zero-pressure-gradient flow with freestream velocity $U_\infty = 5.9$ m/s and $Re_\tau = 1160$ ($Re_\tau = \delta U_\tau/\upsilon$ where δ is the boundary layer thickness, U_τ is the skin friction velocity and υ is the kinematic viscosity of the fluid). The Reynolds number based on the momentum thickness Re_θ was 2808 and the value of δ in the region of the measurement planes was 70.8 mm. The streamwise, spanwise and wall-normal directions are along the x, y and z axes respectively and the fluctuating velocity components along those three directions are represented as u, v and w. All quantities are normalized using "wall" variables U_τ and υ and are denoted with a superscript +.

The experiments conducted used a three-camera polarization-based dual plane PIV system. The setup consisted of two independent PIV systems which captured images of olive oil droplets of size ~1μm. The first system is a stereoscopic setup which is used to measure all three velocity components within a plane, while the second system is a conventional PIV system that measures the in-plane velocity components in a neighboring plane located 21 wall units above in the wall normal direction. Simultaneous measurements were performed in the two planes by using the polarization property of laser light sheets to isolate one camera system from the other[6,8]. Further details of the experimental setup can be found in Ganapathisubramani et al.[5] The experiments here were conducted in the logarithmic region of the turbulent boundary layer, with the first plane located 110 wall units from the wall.

The vector fields for the *1k* x *1k* cameras were obtained using the adaptive central difference technique of Wereley & Meinhart[13]. To obtain the vector fields, the images obtained from PIV were interrogated using a two-frame cross-correlation algorithm with discrete window offset. Firstly, using coarse 64 x 64 pixel windows, the mean displacement for each window was calculated. Next, with a coarse 32 x 32 pixels window and the second window offset by the mean displacement, a vector field was obtained. This image was again interrogated using a 16 x 16 pixel window. At this step, the interrogation box in frame 1 was offset upstream and the frame 2 box was offset downstream by half the mean displacement calculated in the previous step. Thus, the final interrogation window size was 16 x 16 pixels and a 50% overlap was used. The final vector fields obtained from the stereo PIV had a total size of 1.1δ x 1.1δ and the spacing between the vectors was 12.76 x 12.76 wall units. The data from the two planes are used to compute the entire velocity gradient tensor in the lower plane. For the in-plane gradients, a second-order central difference scheme was used, while a first-order forward differencing scheme was used to calculate the streamwise and spanwise velocity gradients in the wall-normal direction. Finally, the wall-normal gradient of the

wall-normal velocity was recovered from the continuity equation. Thus the complete velocity gradient tensor was obtained using this experimental technique.

The DNS dataset under consideration here is a numerical simulation of a fully developed channel flow performed by del Álamo et al.[3] The numerical technique involves the integration of the Navier-Stokes equations in the form of evolution problems for the wall normal vorticity and the Laplacian of the wall-normal velocity. This is the same method as described by Kim et al.[9]. For spatial discretization, Chebychev polynomials are used in the wall normal direction, while de-aliased Fourier expansions are utilized in wall-parallel planes. The temporal discretization used is a third-order semi-implicit Runge-Kutta scheme. Further details of the DNS can be found in del Álamo et al.[3]. The simulation of interest in the present study has a friction Reynolds number of $Re_\tau = 934$, which is referred to as L950. The computational domain in this simulation was $8\pi h$ units in the streamwise direction and $3\pi h$ units in the spanwise direction, where h is the channel half width. The sizes of the domain were set to try to account for all the energy containing structures in the flow, especially features with dimensions of the order of h. The spacing between the vectors was 11.46 x 5.73 wall units in the streamwise and spanwise directions respectively after de-aliasing. This DNS dataset is used to assess the dual plane PIV data extracted experimentally.

3
Averaging techniques used

As described in section 2, the resolution of the DNS dataset is higher than the PIV dataset. In order to obtain comparable resolutions in the two datasets, we need to implement an averaging scheme on the DNS data. The averaging technique is described as follows. The PIV field has a total size of 1.1δ x 1.1δ and it contains a total of 100 x 100 interrogation windows. This yields a field of 100 x 100 vectors, with a spacing of 12.76 wall units between vectors in both the streamwise and the spanwise directions. However, taking into account the overlap of the interrogation windows in the PIV processing, the effective size of the square interrogation window is 25.52 x 25.52 wall units. As described earlier, the spacing between the vectors in the DNS dataset is 11.46 x 5.73 wall units in the streamwise and the spanwise directions. Thus, the aim is to average the DNS values within the appropriate square interrogation windows to obtain a vector field of 100 x 100 points.

One time step of the DNS dataset contains 2048 x 1536 points in the streamwise and the spanwise directions respectively. This large field available from the DNS dataset can be divided into smaller fields of 111 x 222 points in the streamwise and spanwise directions respectively to obtain fields that have a dimension of 1272 x 1272 wall units each, which is almost the same size as the PIV field of 1276 x 1276 wall units. Then, the fields of 111 x 222 points are averaged down to 100 x 100 points to reduce the resolution of the DNS dataset to that of the PIV. We obtain 108 fields of 111 x 222 points from one plane of the DNS dataset and all the fields are processed for statistical analysis.

In the wall normal direction, the laser sheet has a finite thickness. Burn tests were used to estimate the thickness of the laser sheet before the experiments. These tests showed the thicknesses of the laser sheets to be 0.35mm and 0.45mm for the stereoscopic and the single camera systems respectively. This corresponds to 5.6 and 7.2 wall units respectively. Given this configuration of the PIV dataset, the aim is to extract data from the DNS at the corresponding wall normal locations. In the DNS dataset, since Chebychev polynomials are used in the wall normal direction, the spacing between the planes is not uniform. We need to identify wall normal planes which correspond to the PIV data planes.

We use two averaging techniques here. In the 2D averaging technique, we average over a two dimensional window where we reduce the resolution in the streamwise and the spanwise directions only. In the 3D averaging technique, we average over a three dimensional window to also include the effect of averaging in the wall normal direction to account for the thickness of the laser sheet. Both averaging techniques can be used to estimate the effect of the separation between the laser sheets. In both methods, the streamwise-spanwise averaging is implemented as follows. A box of size 25.4 x 25.4 wall units is used to detect all data points that lie within the corresponding interrogation window. This box is moved through the entire field of 111 x 222 points to reduce it to 100 x 100 points. On average, this procedure results in about 4 points per box in the spanwise direction and 2 points per box in the streamwise direction. A simple average is performed to come up with a representative value for each box. This procedure is performed for all three velocity components u, v and w. In case of the 2D averaging technique mentioned above, we average in the streamwise-spanwise plane only, while in the 3D averaging technique, we average in the wall normal direction as well and all points detected within a three dimensional volume are averaged to obtain each velocity component.

In the DNS dataset, the plane numbers 60, 61, 62, 66 and 67 correspond to wall normal locations of 106.738, 110.313, 113.943, 129.012 and 132.914 wall units respectively. For 3D averaging, the planes used are 60, 61 and 62

for plane 1 and planes 66 and 67 for plane 2, while for 2D averaging, only planes 61 and 67 are used. The averaging scheme above is implemented on these planes and this averaged data is analyzed similar to the PIV data.

To calculate the gradients in the raw DNS dataset, a second-order finite difference scheme is implemented in all three directions. For wall normal gradients, information from planes 60, 61 and 62 is used. On the other hand, in the case of the averaged DNS obtained from either averaging technique, the appropriate averaging as described earlier is performed to yield averaged planes 61 and 67. These averaged planes are used to calculate in-plane gradients to second-order accuracy and wall-normal gradients to first-order accuracy using a forward difference scheme. This essentially mimics what happens with the PIV dataset.

4
Results

The averaging techniques described earlier were implemented on the DNS dataset. The instantaneous and statistical results from the dual plane PIV, the raw DNS and the averaged DNS datasets are presented in this section. Some instantaneous velocity and velocity gradient fields are also presented to provide a view of the structure of the turbulent boundary layer. The mean and r.m.s. statistics of the velocity and vorticity components computed from the dual plane PIV, raw DNS dataset and the 3D averaged DNS dataset are listed in Table 1. As expected, the averaging reduces the r.m.s. values of the DNS dataset.

The mean and r.m.s. values of the DNS are comparable to those of the PIV dataset. The values of wall normal gradients present in ω_x and ω_y are better resolved in the case of the raw DNS since they are computed with second order accuracy.

	$\overline{U}^+$	σ_u^+	σ_v^+	σ_w^+	$\sigma_{\omega_x}^+$	$\sigma_{\omega_y}^+$	$\sigma_{\omega_z}^+$	$\overline{\partial U^+ / \partial y^+}$	λ_{3D}^+
PIV data	16.04	1.91	1.34	1.16	0.069	0.064	0.055	0.0022	0.0382
Raw DNS	16.67	1.89	1.06	1.33	0.081	0.070	0.075	0.0022	0.0302
Averaged DNS	16.67	1.84	0.98	1.27	0.053	0.053	0.052	0.0019	0.0216

Table 1: Ensemble averaged flow mean and r.m.s. (root mean square) statistics from dual-plane PIV, raw DNS and averaged DNS datasets. $\sigma_{\omega_x}^+, \sigma_{\omega_y}^+ \& \sigma_{\omega_z}^+$ are the r.m.s. of the fluctuating vorticity components.

Instantaneous contour plots of a sample velocity field are shown in Figure 1. The contours show the instantaneous streamwise velocity U^+ normalized in wall units. The plots show the effects of averaging introduced by implementation of the techniques described earlier. The averaged plots show some smoothing of the velocity contours. It is also apparent that features which are more distinct and sharp in the raw DNS plots appear blurred in the averaged fields. This is as expected from averaging of any kind. From the plots of the derivatives of the averaged velocity fields, it is found that averaging over the wall normal direction, as might occur over a finite laser sheet thickness, does not cause appreciable differences in the values of the derivatives. As a result, we will use only the 2D averaging for further analysis. This difference was checked on various individual in-plane and out-of-plane derivatives as well as on derived quantities such as vorticity and swirl. Figure 2 illustrates this result for one gradient of the streamwise velocity. It must be observed that the plot of the gradient appears different for the raw and the averaged DNS due to the fact that the averaging shifts the local value of the quantity closer to the mean. However, the basic structures observable in the raw DNS can be seen in both the 2D and 3D averaged plots. As shown in Table 1, the mean value of the derivative quantity does not change significantly due to averaging (within the uncertainties of calculation), whereas the mean value of swirl strength is lowered because lesser cores are identified due to averaging and blurring of vortex cores. The mean value of the derivative does not change significantly because the derivative and the ensemble averaging commute linearly, whereas the plots of derived quantities such as swirl change appreciably since the relation between ensemble averaging and the derived quantities is not linear.
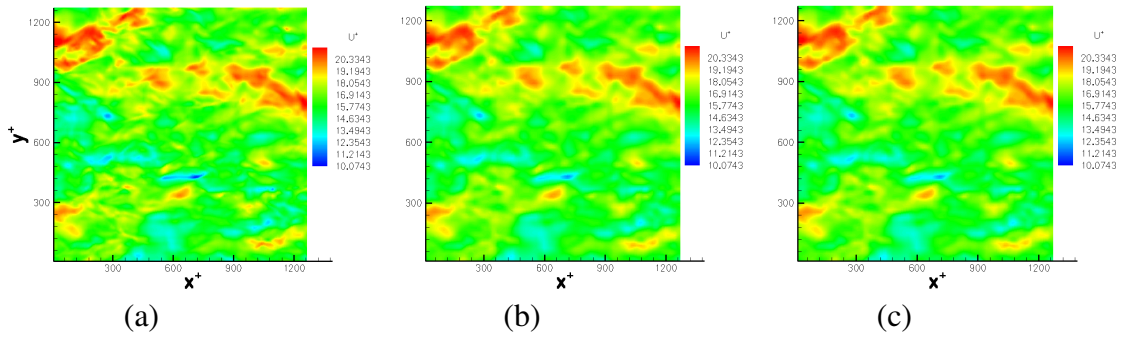
Figure 1: Contour plots of U^+ (a) Extracted from raw DNS data. (b) Extracted from 2D averaging (c) Extracted from 3D averaging
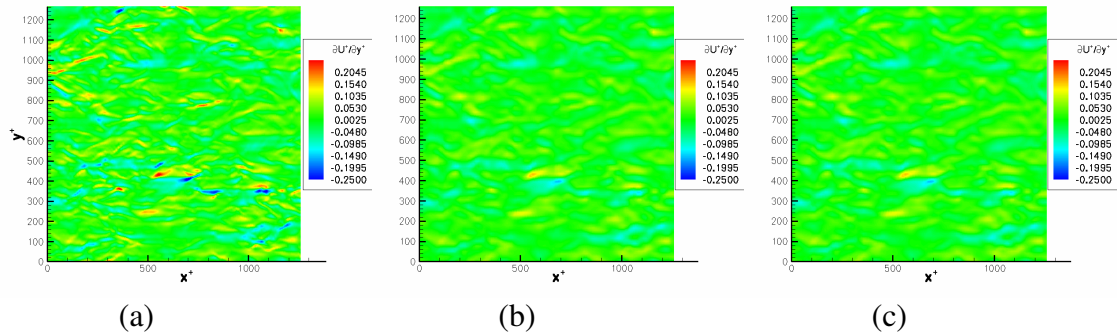

Figure 2: Contour plots of $\partial U^+ / \partial y^+$ (a) Extracted from raw DNS data. (b) Extracted from 2D averaging (c) Extracted from 3D averaging

Thus, more noticeable differences are observed in the plots of the two dimensional and three dimensional swirl strengths shown in Figures 3 and 4. The two-dimensional swirl strength λ_{2D}^+ is generally defined as the imaginary part of the complex root of the characteristic equation of the two dimensional velocity gradient tensor (Adrian *et al.*[2]). λ_{2D}^+ is an indicator of the presence of regions of fluid swirling about an axis aligned with the wall normal direction. In the present case however, the three dimensional swirl strength λ_{3D}^+ can be calculated from the full velocity gradient tensor. Zhou *et al.*[14] suggested the use of the imaginary part of the complex eigen value (λ_{ci}) of the full velocity gradient tensor to visualize vortices. λ_{3D}^+ is an indicator of the presence of regions of fluid swirling about any axis, not necessarily perpendicular to the wall. Explicit definitions of swirl can be found in Ganapathisubramani[6]. Mathematically, λ_{3D}^+ is greater than or equal to λ_{2D}^+, depending on the deviation of the swirling motion from the wall-normal direction.

By comparing the plots from raw and averaged DNS in Figures 3 and 4, we can see that structures which appear sharper in the raw DNS are blurred and less resolved in the averaged DNS. One effect of this is that the sizes of the vortex cores appear larger in the averaged fields. The number of vortex cores identified also decreases on averaging, which has an impact on the statistics derived from the swirl fields. The following section will discuss the statistical results obtained from the instantaneous swirl fields and implications on the probable structure of vortices.
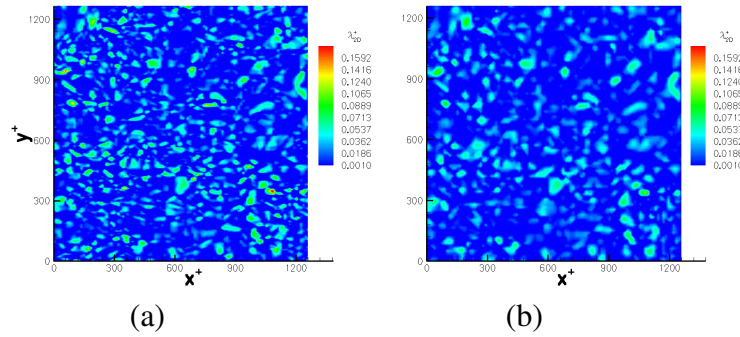
(a)   (b)

Figure 3: Contour plots of λ_{2D}^+ (a) Extracted from raw DNS data (b) Extracted from averaged DNS data

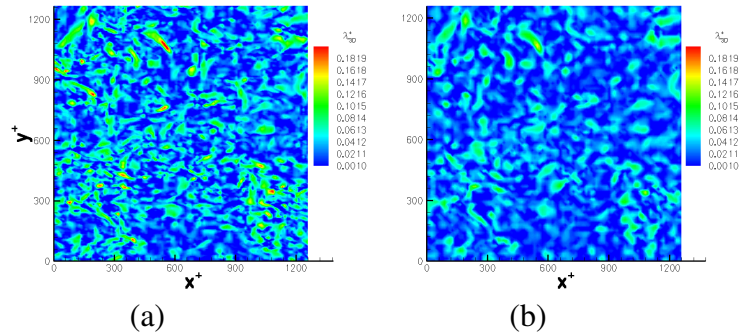(a)   (b)

Figure 4: Contour plots of λ_{3D}^+ (a) Extracted from raw DNS data (b) Extracted from averaged DNS data.

5
Vortex structure deduced from instantaneous results

An average or probable structure of a hairpin vortex can be deduced from statistics derived from the instantaneous swirl strength fields. The complete velocity gradient tensor can be used to compute the inclination angle of any individual vortex structure by determining the orientation of the vorticity vector averaged over the region of the vortex core. The aim of averaging the vorticity vector over the region of the vortex core is to annul the effects of small scale variations in the local vorticity vector.

The region growing algorithm used to identify vortex cores is discussed in detail in Ganapathisubramani *et al.*[4] & Ganapathisubramani[6]. However, it is also briefly described below. The aim is to identify connected points of swirl strength greater than a certain determined threshold. The algorithm identifies all local maxima of λ_{3D}^+ in the field greater than the threshold. This threshold was fixed at 10% of the maximum value in the data set in order to filter out contributions from weak vortex structures and measurement noise. These points were then used as seed points for a region growing algorithm that identifies a connected region of swirl with values greater than the threshold. In order to again reduce contributions from measurement uncertainty and other noise, a lower limit on the minimum number of points included in a connected region is also imposed. The choice of this threshold is crucial to the functioning of the algorithm, and its effect on the statistical distribution is discussed in detail later. For the present study, this threshold is fixed at 12 points for the raw DNS and 5 points in the average DNS & PIV datasets. These numbers are chosen based on the spatial grid sizes in the different datasets to use the same threshold on area occupied by the core. Once the core regions have been identified, the average values of the three components of vorticity are computed in the connected regions. An additional constraint which is imposed is that the average value of at least one vorticity component must be greater than the standard deviation of that component for that core to be included in a distribution of a related core angle. Also, a given projection angle is computed only if the average vorticity value of at least one component used in its computation is greater than its standard deviation. These criteria essentially eliminate contributions to the probability density function (p.d.f.) of specific projection angles from weak vorticity values. Figure 5 shows a sample swirl field and the results of the vortex core identification algorithm. Two thresholds on the number of points are used in the results shown. It must be noted that the sizes and shapes of the identified cores agree well with locations of significant swirl. A higher threshold on the number of points also

ensures that only stronger cores with greater circulation are identified as the average vorticity exceeds the vorticity threshold.
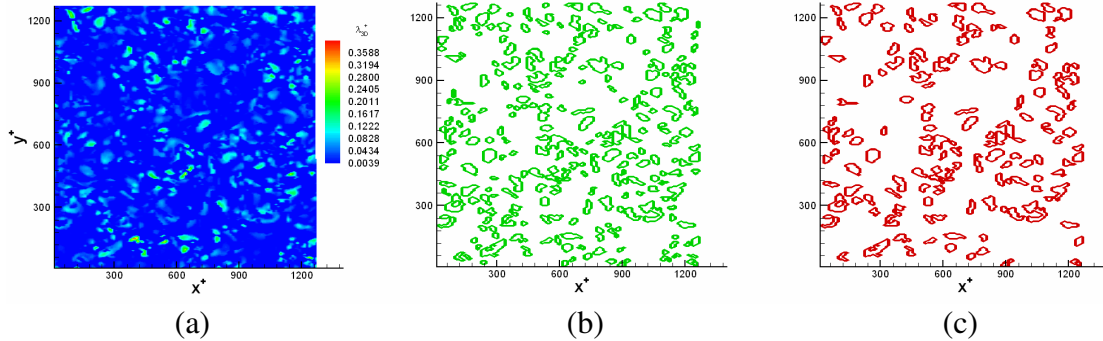

<div align="center">(a)   (b)   (c)</div>

Figure 5: Performance of the vortex core identification algorithm for raw DNS data.
(a) λ_{3D}^+ . Cores identified with (b) 5 point threshold (c) 12 point threshold

Figure 6 shows the p.d.f. of the elevation angle θ_e made by the vortex cores for the raw DNS and the PIV datasets. The elevation angle, which is defined as the angle made by the vorticity vector with the *x-y* plane, can vary from -90° to +90°. The distribution, shown by square symbols in both the PIV and DNS datasets, shows that a large percentage of structures have very low elevation angles. This suggests that these contributions are made by structures in planes parallel to the wall i.e. streamwise and spanwise structures oriented in the plane of measurement. In order to obtain the inclination angles of cores that are not in the streamwise-spanwise planes, we need to filter out these in-plane structures. It is here that the two-dimensional swirl is useful. λ_{2D}^+ can be used to identify structures swirling about an axis perpendicular to the wall parallel plane. Thus the use of λ_{2D}^+>0 as an additional constraint provides us with a means of identifying only out of plane structures. The resulting curves are also plotted in Figure 6. Both the DNS and the PIV datasets seem to provide consistent results, and the peaks of the curves of λ_{3D}^+ (λ_{2D}^+>0) lie at about 40°. Further, the curve shapes seem to suggest that most of the structures are inclined at angles between 25° and 50° to the wall parallel plane. In all further p.d.f. plots of vortex angles, the criterion λ_{2D}^+>0 is enforced.
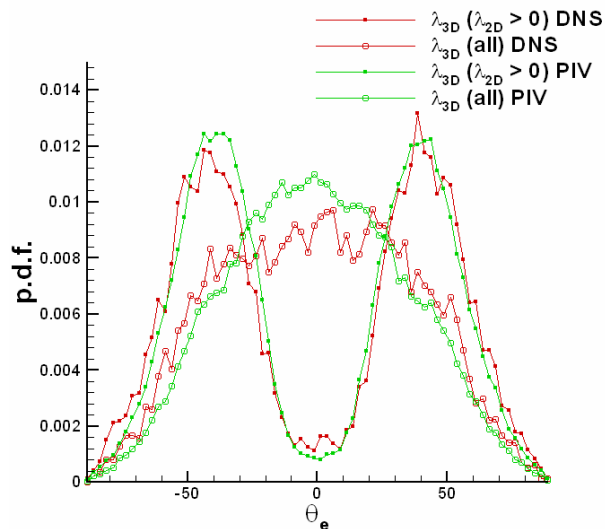

Figure 6: p.d.f. of the elevation angle θ_e for the raw DNS and the PIV datasets

The projection angles of the vortex structures in the *x-z*, *x-y* and *y-z* planes are calculated using the projections of the vorticity vector in the respective planes. Firstly, the probability distribution of the inclination angle θ_{xz}, which is the angle made by the projection of the vorticity vector in the *x-z* plane with the positive *x*-axis, is shown in Figure

7(a). In this plot, the results from the raw DNS, the averaged DNS and the PIV datasets are plotted. The plots indicate peaks close to $\theta_{xz}=45°$ and -135°. The peaks are consistent with the presence of positive and negative legs of a forward-leaning hairpin vortex. Another interesting observation is the fact that there is a finite probability of θ_{xz} lying between -90° & 0° and 90° & 180°, which suggests the presence of backward leaning structures. Both the PIV and the DNS data consistently seem to suggest the above results. Comparing the averaged DNS data to the PIV and the raw DNS data, it is observed that the averaging gives results which are really close to those predicted by either method and are within the range of the accuracy of the measurements and the feature extraction scheme.
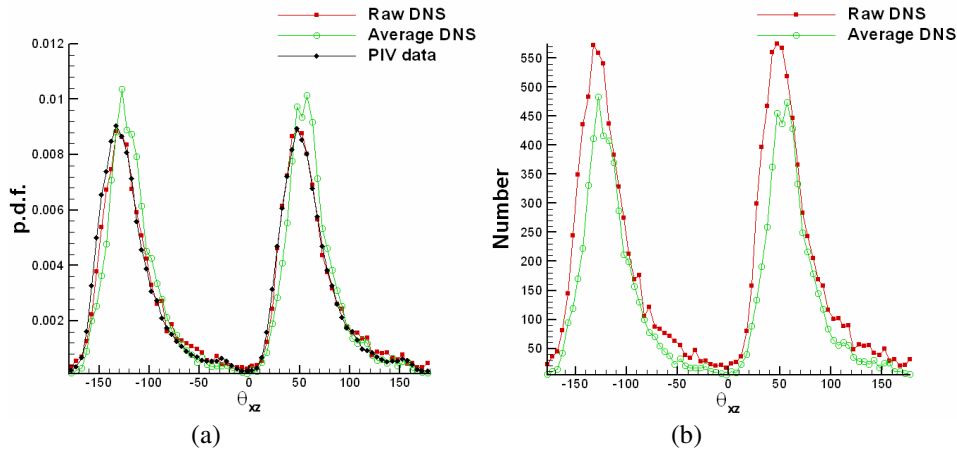

Figure 7: (a) p.d.f. of θ_{xz} from raw DNS, average DNS & PIV. (b) Absolute number of cores identified at each angle from raw & average DNS datasets.

As can be seen from the plot, the effect of averaging is to slightly increase the probability of the angle of inclination to lie in the range of 25° to 50°. Figure 7(b) illustrates how this occurs. The averaging almost uniformly cuts off vortex cores from all the possible angles of inclination from -180° to +180°. The effect of this is what is seen in Figure 7(a), by which the probability of occurrence of forward leaning structures in the averaged DNS is higher than in the raw DNS dataset. Although the raw DNS also indicates that the boundary layer is dominated by forward leaning structures, the plot might suggest that the averaging introduced in this case causes the probability of occurrence of forward leaning structures to appear more than in reality. However, the most significant observation from this is that results from both the raw and the averaged DNS data match the PIV results almost exactly qualitatively and within acceptable variations quantitatively.

Figure 8 illustrates the effect of the thresholds on the minimum number of points per core identified. The effect of this constraint is that smaller and, in general, weaker cores are filtered out by increasing the minimum number of points. The other advantage of using a higher threshold is that it reduces identification of measurement noise as vortex cores. On the other extreme, a very high threshold could impose too stringent a constraint and might prevent identification of genuine vortex cores. So a balance has to be struck in the choice of this threshold.

The eddy inclination angle θ_i, which is computed under the assumption that eddies are symmetric hairpins about an *x-z* plane, is defined as the single angle that represents the inclination of the eddy with respect to the *x-y* plane. To obtain this, we accumulate all the forward leaning eddies together and all the backward leaning eddies together. The resulting p.d.f. is shown in Figure 9(a), and the absolute number of vortex cores versus the eddy inclination angle is shown in 9(b).
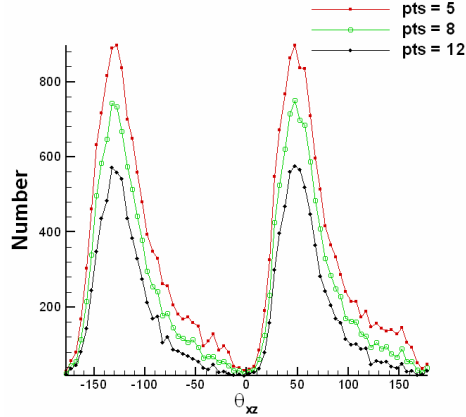
Figure 8: Absolute number of cores identified for different thresholds on the minimum number of points per core identified for the raw DNS data.
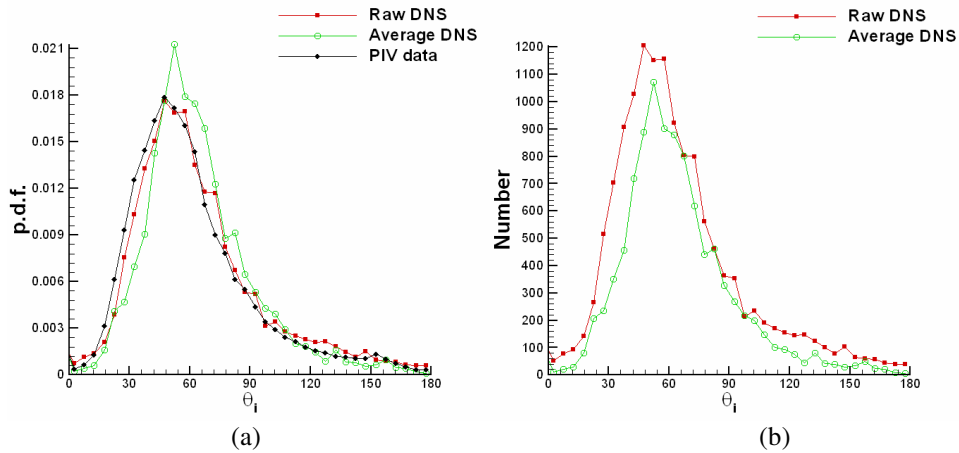

(a)　　　　　　　　　　　　　　　(b)

Figure 9: (a) p.d.f. of θ_i from raw DNS, average DNS & PIV. (b) Absolute number of cores identified at each angle from raw & average DNS datasets.

As was observed with the plots of θ_{xz} and θ_i, the effect of averaging seems to reduce the absolute number of cores of all the possible angles of inclination. However, the qualitative agreement in this case is also almost exact and the good quantitative agreement suggests that the predictions of the PIV and the DNS datasets are almost identical.

The projections of the vorticity vector on the other planes can be used to further understand the typical structures in the turbulent boundary layer. The angle made by the projection of the vorticity vector on the *x-y* plane with the positive y-axis is referred to as θ_{yx} and the angle made by the projection on the *y-z* plane with the positive y-axis is referred to as θ_{yz}. These are shown in Figures 10(a) and 10(b) respectively.

In the PIV data, the p.d.f. of θ_{yx} shows the existence of three peaks. The main peak occurs at 0°. If we assume that the field is dominated by hairpin structures, this could be caused by the regions around the heads of the hairpin loops. The other two peaks are located at θ_{yx} = 75° and -75° and these could be caused by the positive and negative 'Λ' shaped necks of a hairpin vortex. The averaging once again seems to cause a slight increase in the probabilities of occurrence of structures close to the peaks. The raw DNS dataset seems to suggest the presence of a higher number of structures in the range θ_{yx}>120° and θ_{yx}<-120° than predicted by the PIV data.
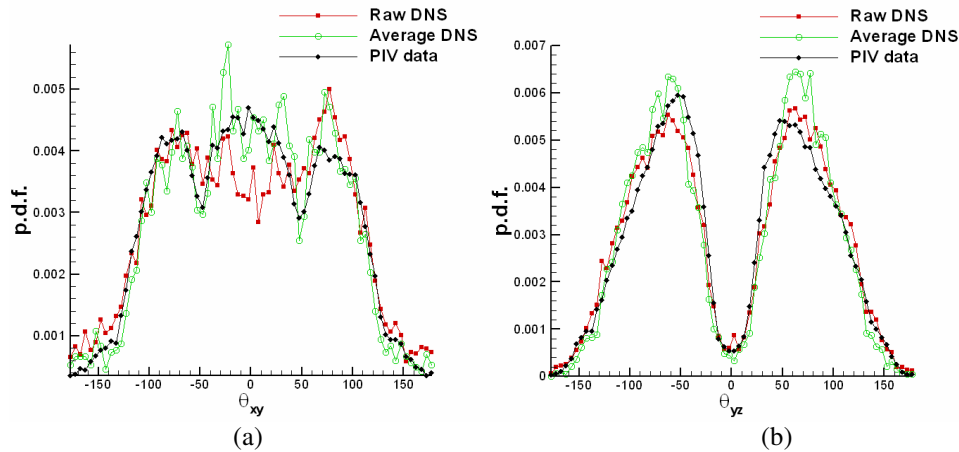
9

Figure 10: (a) p.d.f. of θ_{yx} (b) p.d.f. of θ_{yz}

The p.d.f. of θ_{yz} are more closely matched for the raw DNS, the averaged DNS and the PIV data compared to the other angles. θ_{yz} is the angle made by the projection of the vorticity vector on the *y-z* plane with the positive y-axis. The PIV data predicts peaks close to 45° and -45°, and both the raw and the averaged DNS datasets predict almost the same values for the peaks. As observed with earlier quantities, good qualitative and quantitative agreement between the different datasets is observed.

6
Conclusions

The vortex distribution in the turbulent boundary layer is analyzed using statistical tools applied on an experimental dataset from a dual plane PIV system and a DNS dataset in a channel. The effect of averaging on the DNS is studied and is analyzed as a possible interpretation of PIV. The effect of averaging seems to be a prediction of a slightly higher probability of occurrence of forward leaning hairpin structures, due to the reduction in the number of vortex cores identified as observed with the absolute number plots. Averaging also seems to filter out the small scale structures from the field. This averaged data gives us a good idea of stronger structures expected to drive dynamical interactions within the boundary layer. However, most importantly this serves as strong validation for the experimental technique and convincingly demonstrates that such PIV data can be used to assess information related to velocity gradients and to characterize vortical structures. It clearly illustrates that the effect of averaging does not affect the angle statistics either qualitatively or quantitatively. For this study, only one large domain from one time setp of the DNS was used. It is expected that the use of more data fields from the DNS to attain statistical convergence will further illustrate the close match between the experimental and numerical datasets.

7
Acknowledgements

8
References

1. **Adrian, R.J., Christensen, K.T. & Liu, Z.C.** (2000) Analysis and interpretation of instantaneous turbulent velocity fields. *Exp. Fluids* 29, 275-290
2. **Adrian, R.J., Meinhart, C.D. & Tomkins, C.D.** (2000) Vortex organization in the outer region of the turbulent boundary layer. *J. Fluid Mech.* 422, 1-53
3. **del Álamo, J.C., Jiménez, J., Zandonade, P. & Moser, R.D.** (2004) Scaling of the energy spectra of turbulent channels. *J. Fluid Mech.* 500, 135-144.

4. **Ganapathisubramani, B., Longmire, E.K. & Marusic, I.** (2005) Investigation of structural properties of hairpin type vortices in a turbulent boundary layer. *Phys.Fluids.*, in preparation.

5. **Ganapathisubramani, B., Longmire, E.K., Marusic, I. & Pothos, S.** (2005) Dual-plane PIV technique to determine the complete velocity gradient tensor in a turbulent boundary layer. *Exp. Fluids,* In press.

6. **Ganapathisubramani, B.** (2004) Investigation of turbulent boundary layer structure using stereoscopic particle image velocimetry. Ph.D. thesis, University of Minnesota, USA.

7. **Ganapathisubramani, B., Longmire, E.K. & Marusic, I.** (2003) Characteristics of vortex packets in turbulent boundary layers. *J. Fluid Mech.* 478, 35-46.

8. **Kahler, C.J.** (2004) Investigation of the spatio-temporal flow structure in the buffer region of a turbulent boundary layer by means of multiple plane stereo PIV. *Exp. Fluids* 36,114-130.

9. **Kim, J., Moin, P. & Moser, R.** (1987) Turbulence statistics in fully developed channel flow at low Reynolds number. *J. Fluid Mech.* 177, 133-166.

10. **Moin, P. & Mahesh, K.** (1998) Direct Numerical Simulation: A tool in turbulence research. *Annu. Rev. Fluid Mech.* 30, 539-78.

11. **Raffel, M., Willert, C. & Kompenhans, J.** (1998) Particle Image Velocimetry – A practical guide. *Springer-Verlag.*

12. **Theodorsen, T.** (1952) Mechanism of Turbulence. *Proc. Second Midwestern Conference on Fluid Mechanics*, Mar 17-19. Ohio State University, Columbus, Ohio.

13. **Wereley, S.T. & Meinhart, C.D.** (2001) Second-order accurate particle image velocimetry. *Exp. Fluids* 31, 258-268.

14. **Zhou, J., Adrian, R.J., Balachandar, S. & Kendall, T.M.** (1999) Mechanisms for generating coherent packets of hairpin vortices in channel flow. *J. Fluid Mech.* 387, 353-396.